



## Supplementary Materials for

### **A 3D-printed, functionally graded soft robot powered by combustion**

Nicholas W. Bartlett,\* Michael T. Tolley, Johannes T. B. Overvelde, James C. Weaver,  
Bobak Mosadegh, Katia Bertoldi, George M. Whitesides, Robert J. Wood

\*Corresponding author. E-mail: [nbartlett@seas.harvard.edu](mailto:nbartlett@seas.harvard.edu)

Published 10 July 2015, *Science* **349**, 161 (2015)  
DOI: 10.1126/science.aab0129

#### **This PDF file includes:**

Materials and Methods  
Supplementary Text  
Figs. S1 and S2  
Table S1  
Captions for Movies S1 and S2

**Other Supplementary Materials for this manuscript include the following:**  
(available at [www.sciencemag.org/content/349/6244/161/suppl/DC1](http://www.sciencemag.org/content/349/6244/161/suppl/DC1))

Movies S1 and S2

## Materials and Methods

The Stratasys website provided general information regarding the 3D printed material used in this project (specifically, the “PolyJet Materials Data Sheet” and the “Digital Materials Data Sheet”). Published data sheets indicate that the materials used in the robot ranged in hardness from Shore A 27 to Shore D 83. We performed additional analysis of the 3D printed material through different tests on a universal testing machine (Instron 5544, Instron). Cyclic testing indicated that at high rates of extension, significant hysteresis was present due to the viscoelastic properties of the 3D printed material. However, at rates below 0.03125 mm/s, all viscous effects were negligible and the material behaved elastically. Each of the nine different materials used in the stiffness gradient was tested in a standard tensile test (ASTM D 638, Type IV), performed at 0.03125 mm/s to eliminate any rate dependent behavior. From this test, we obtained values for the shear and Young’s moduli of each material, which were subsequently used in the simulations. The material properties can be found in Table S1.

We conducted extension tests on samples that featured either an abrupt transition from the softest to the most rigid material or a more gradual step-wise transition by incorporating materials of intermediate moduli. In fatigue tests in which we repeatedly stretched the samples to an extension of 5 mm (20% of the test section) at 0.03125 mm/s, the discrete samples failed after an average of 436 cycles, whereas the gradient samples lasted an order of magnitude longer (most samples were discontinued after 24 hours of testing, over 8640 cycles).

We designed the robots using SolidWorks, a 3D computer aided design (CAD) software, and printed them with a multimaterial 3D printer (Connex500, Stratasys Ltd.). The body was printed as a single piece. We cleared residual support material from the 3D printing process through a small excavation hole using a high pressure washer (Powerblast High Pressure Water Cleaner, Balco UK). After clearing all of the support material, we sealed the excavation hole by attaching a custom 3D printed cap to the body with cyanoacrylate adhesive (Loctite 416, Henkel AG & Company, KGaA).

In addition to the custom fabricated body, the robot consisted of a number of off-the-shelf components. These include a lithium polymer battery (E-flite 180 mAh 2S 7.4V 20C, Horizon Hobby Inc.), a mini-diaphragm pump (KPV-14A, Clark Solutions), six miniature pneumatic solenoid valves (X-Valve, Parker Hannifin Corp.), a butane fuel cell (RC-31, Master Appliance Corp.), and a pressure regulator (PRD-2N1-0-V, Beswick Engineering Co.). Oxygen was stored in a repurposed 16g CO<sub>2</sub> cartridge, outfitted with a piercing fitting (GCP-1038-3V, Beswick Engineering Co.) and ball valve (MBV-1010-303-V, Beswick Engineering Co.). The high voltage source was obtained from components of a continuous ignition gas lighter (57549 Olympian GM-3X Gas Match, Camco Manufacturing Inc.). The circuit board was custom designed with an Atmel ATmega168 microcontroller, and was programmed using the Arduino IDE.

The timing sequence on the solenoid valves determined how much butane and oxygen was delivered to the combustion chamber. After fixing the settings on both the pressure regulator (which was in-line with the oxygen cartridge) and the valve of the butane fuel cell, we determined flow rates of oxygen and butane by opening the respective valves for a predetermined amount of time and measuring the amount of gas delivered by bubbling into an inverted graduated cylinder. This procedure was repeated throughout the testing period to ensure consistency.

The first step in the testing procedure was refilling the butane fuel cell (if necessary) and refilling the oxygen cartridge. The oxygen cartridge was filled from a supply tank of oxygen regulated to 90 psi, and then sealed using the ball valve. It was then threaded into the regulator on the robot, keeping the ball valve closed until the initiation of a new test. Due to the rapid use of oxygen, five oxygen cartridges were filled and used during each testing cycle.

We explored the space of butane to oxygen ratios extensively during testing, and found a baseline mixture of 50 mL of oxygen and 24 mL of butane per jump to be the most consistent. The volume of the oxygen cartridges and the filling pressure limited the number of jumps on a single cartridge to two (or three if the amount of fuel delivered was reduced appropriately).

The circuit board was designed to run the same program each time the robot was turned on. Adjustments to the program required plugging the circuit board directly into a computer and opening the Arduino IDE.

Experiments were recorded using both a DSLR camera (D600, Nikon Inc.) and a high-speed camera (Phantom v710, Vision Research Inc.). The latter was run at 1000 or 2000 frames per second and operated using Phantom Camera Control (PCC) software. For Figures 3B and 3C, the multiple video frames were background subtracted and merged using Adobe Photoshop (Adobe Systems).

Non-linear finite element analysis was performed using the commercial package Abaqus/Explicit (v6.12) (Abaqus Unified FEA, Dassault Systemes). All materials were modeled using a Neo-Hookean material model (27), each with a specific initial shear modulus. The shear moduli were determined experimentally by performing uniaxial tension tests and fitting the stress-strain curves using a least squares approximation.

To qualitatively show the effect of using materials with different moduli within the same structure, we deformed three beams with a different material distribution by twisting them 180 degrees. These beams were modeled using approximately 10,000 tetrahedral elements (Abaqus element code C3D4), and quasi-static conditions were assured by using a relatively long simulation time, as well as a small damping factor (Fig. 2A).

We simulated the behavior upon pressurizing the internal cavity of the robot, neglecting the dynamic effects that occur in experiments when actuating the robot. Instead, we ensured quasi-static conditions to generate smoother results that enable a better comparison between the different designs of the top hemispheroid. We modeled the hemispheroid using the same shear moduli as used for the beams, but to reduce computation time we used approximately 50,000 triangular shell elements (Abaqus element code S3R), instead of using solid tetrahedral elements. In the simulations, we fully account for contact between all faces of the model. We inflated the internal cavity by using the surface-based fluid cavity capability in Abaqus, and monitored the pressure during inflation. To determine the force that was generated during inflation, we fixed the top center of the top hemispheroid (1 cm diameter) and measured the vertical reaction force during inflation.

To determine the forces generated during impact, we used the same conditions as those used in inflation. All dynamic effects were neglected; instead the robot was slowly forced into the ground by displacing the top center of the top hemispheroid (1 cm diameter) down towards the ground, while monitoring the reaction force in the upward direction.

## Supplementary Text

At a high level, we acknowledge that the design space is large, and that there are many good designs to meet the requirements of a jumping robot powered by combustion. The robot presented by Loepfe et al. (26) provides an example of an alternative design to a similar problem. The roly-poly geometry enabled their robot to recover from landing in any orientation and to be ready for the next jump. Our system featured a geometry that, while unable to recover from certain landing orientations, was able to control jump direction. Incidentally, it is interesting to see that they independently settled on the power actuator design of an inflated membrane; however, instead of a bistable design, they rely on material strain for membrane deflection. While membrane deflection decreases the power available for jumping, it further aids the robot in returning to its initial jump-ready configuration, as there is just one stable state. The large design space resulted in two designs that differ based on differently prioritized performance requirements. The robot from Loepfe et al. showed consistent, repeatable operation even on rough terrain, while our system demonstrated directional control and good robustness.

We tested multiple robot bodies, as the body design evolved iteratively (which was enabled by the modular design). Early bodies failed upon combustion of the fuel because of stress concentrations from the use of screws to attach the core to the body. When the screws were replaced by mushroom-head fasteners, the main section of the body would only fail under oblique impacts on landing from tests using elevated fuel levels. A common mode of failure was also the tearing of the soft, bottom hemi-ellipsoidal portion of the legs due to repeated inflation/deflation cycles and the poor fatigue properties of the flexible 3D printed material.

In the tests in which we compared the impact behavior of the gradient top robot to the rigid top robot, we dropped the gradient robot, with all of the control components attached, from the maximum height achieved by the rigid top robot. The robot was dropped from numerous orientations to mimic the variability in landing. The gradient top robot survived a total of 35 falls. Unlike the rigid top robot, in which structural failure was catastrophic, the failure mode of the gradient top robot on the 36<sup>th</sup> fall was a cracking of one of the legs, which is easily repairable with a urethane adhesive.

In the baseline testing condition, 50 mL of oxygen was used for each jump. The oxygen cartridge had an internal volume of 20 mL and was pressurized to 90 psi, giving an initial volume of oxygen (at STP) of 122 mL. Thus, there should have been 22 mL left after the two jumps. Measurement of the remaining oxygen showed that  $14.5 \pm 4.2$  mL (N=6) was left. The discrepancy ( $\sim 7.5$  mL) is likely due to inaccuracies in determining the exact valve timing and imperfections in the press fits of the tubing, valves, and connectors.

The supply pressure effect was certainly a factor, as the pressure of the oxygen cartridge changed significantly from the first jump to the second. We accounted for this fact by using different valve timing on the first and second jumps. The correct timing was determined experimentally by (1) filling an oxygen cartridge to standard experimental conditions, (2) opening the valve and noting the time required to deliver 50 mL oxygen, then closing the valve, and (3) reopening the valve a second time to deliver the same amount of oxygen, again noting the (new) time. We found that after filling to 90 psi, a standard 16g CO<sub>2</sub> cartridge would deliver 50 mL of oxygen in 1.95 seconds. The now lower pressure cartridge would deliver the same volume of oxygen (50 mL) in 1.50 seconds upon opening the valve a second time.

Fuel measurements were taken periodically over months of testing, and thus conditions (e.g. ambient temperature, humidity, etc.) varied. As discussed above, the flow rate of oxygen was variable, and so fuel delivery was determined by experimenting with valve timing. For an oxygen cartridge filled to 90 psi, opening the valve for 1.95 seconds delivered  $56.3 \pm 5.8$  mL (N = 15). The second valve opening of 1.50 seconds delivered  $47.5 \pm 2.7$  mL (N = 6). The flow rate of butane was notoriously variable, depending on how much liquid butane was in the container, the orientation of the container, and how forcefully it was press fit into the core module. After a procedure that produced somewhat reliable results was established, we determined a flow rate of  $1.1 \pm 0.4$  mL/s (N = 21).

In tethered experiments on the gradient top robot (in which the control hardware was off-board and thus the robot was significantly lighter), the robot achieved its highest jump of 2.35 m using 50 mL of butane and 120 mL of oxygen. With a body mass of 478.6 g, this jump corresponds to an efficiency of 0.18% (+0.11%, -0.05%). The most efficient jump was a tethered test that reached 1.60 m using 24 mL of butane and 50 mL of oxygen, corresponding to an efficiency of 0.26% (+0.15%, -0.07%). For the untethered system, a robot with a total mass of 964.6 grams jumped 0.76 m using 24 mL of butane and 50 mL of oxygen, corresponding to an efficiency of 0.25% (+0.14%, -0.07%). The amounts of oxygen and butane used for the maximum height jump and most efficient jump did not correspond to calculated stoichiometric ratios. However, given that fuel delivery was quantified by valve timing, the exact amount of butane or oxygen delivered was unable to be precisely determined. In addition, we did not actively remove the preexisting air from the system, meaning that some amount of air was present in the combustion chamber in addition to the delivered amounts of oxygen and butane. Another source of error was the possibility that some of the butane was being absorbed into the walls of the combustion chamber.

Using smaller volumes of butane and oxygen, we were able to achieve multiple successive jumps in the tethered gradient top system. We demonstrated multiple jumps of differing heights (1.00 m jump followed by 0.30 m jump), as well as multiple jumps of roughly the same height (0.15 m and 0.15 m, also 0.50 m and 0.30 m).

As oxygen was the limiting fuel source, additional jumps could have been achieved by increasing the pressure of the stored oxygen. The pressure canister we used had an internal volume of 20 mL and is rated to contain pressures up to 6.2 MPa (900 psi). At this pressure, the canister could hold 1.62 g of oxygen, which is equivalent to 1.22 L at room temperature (20°C) and atmospheric pressure. This amount of oxygen is enough for 32 consecutive jumps. A full butane fuel cell holds 3.3 g of butane, or 1.38 L of gaseous butane at room temperature and atmospheric pressure, or enough for 57 jumps. Thus, oxygen was the limiting fuel. For safety reasons, we used oxygen pressurized to only 90 psi and replaced the oxygen supply after two jumps.

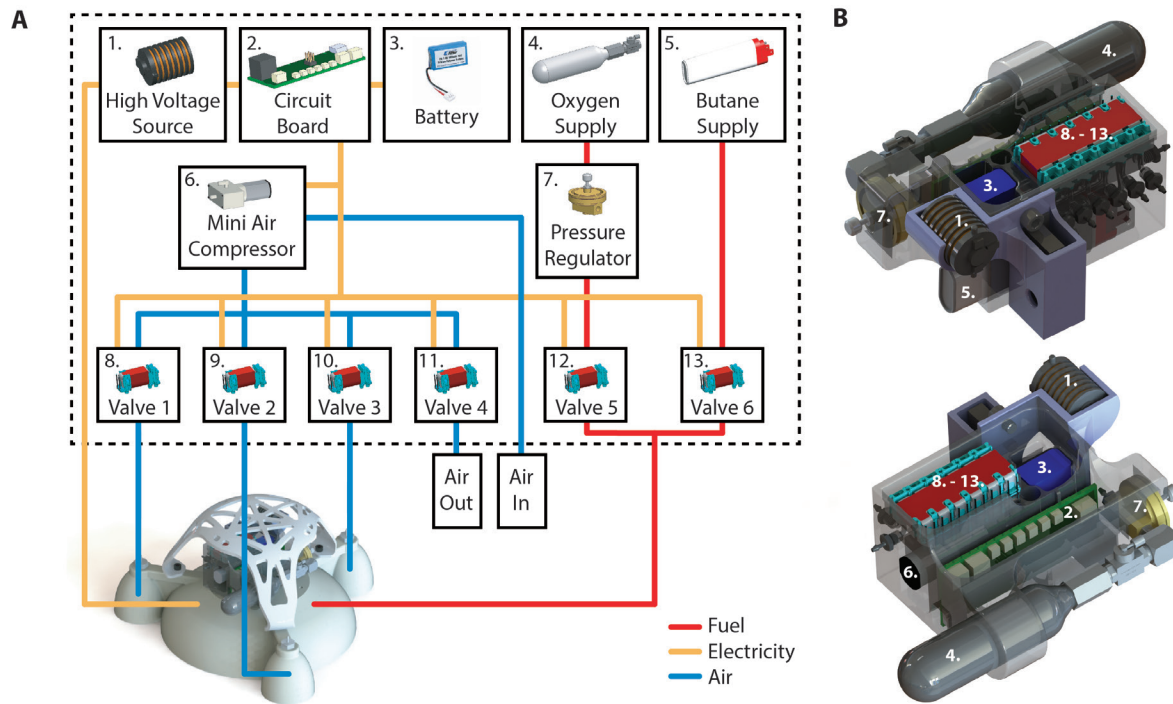


**Fig. S1. Driving components and core module.** (A) Functional dependencies of the control hardware. (B) CAD model of the core module with components from (A) labelled.

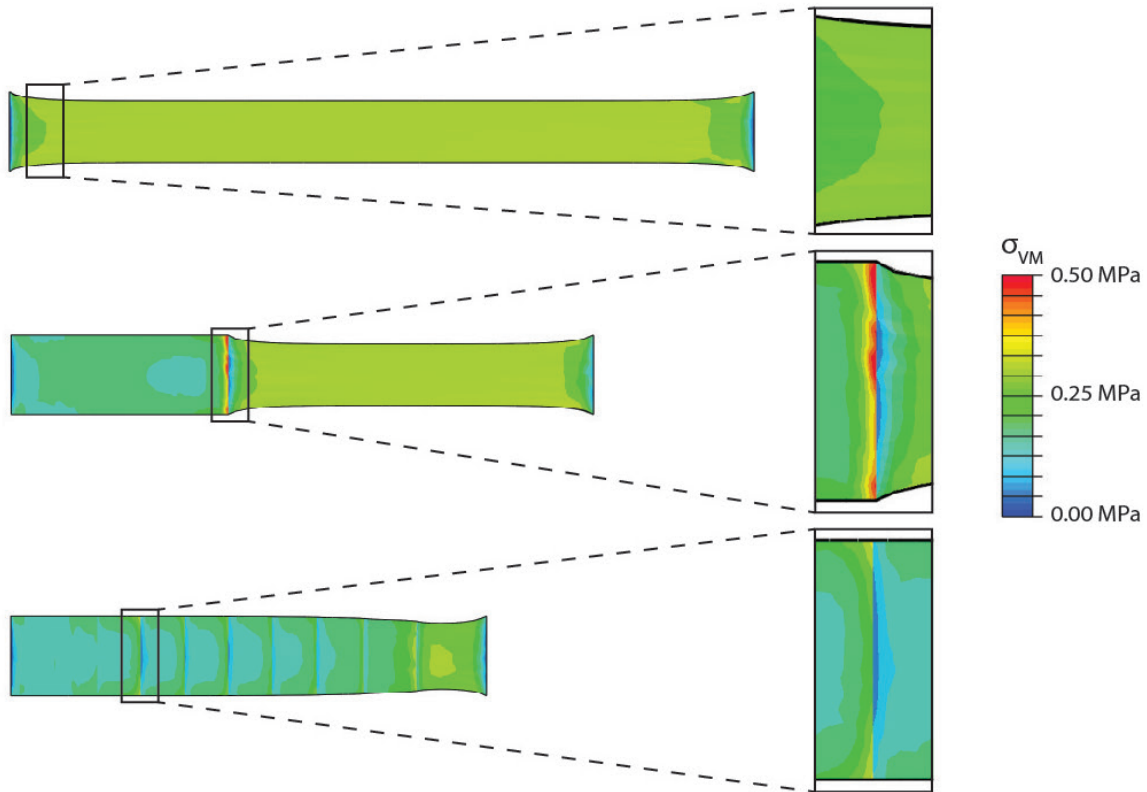


**Fig. S2. Simulations of beams in tension.** Simulations of beams in tension that are fully flexible (top), half rigid and half flexible (middle), and transition gradually from rigid to flexible (bottom). The maximum stresses in each of these beams are 0.35 MPa, 0.54 MPa, and 0.37 MPa, respectively. Compared to the half rigid and half flexible beam, the fully flexible and gradient beams experience maximum stresses of 64.8% and 68.5%, respectively. Simulations were done with (undeformed) beam dimensions of 25.4 mm x 152.4 mm x 1.0 mm. Enlarged images of the points of stress concentration are shown to the right of each beam. Additional motivation for the use of a gradient was derived from considerations of the effect of stress concentrations on interfacial failure in multi-material systems, a problem that is well established in the mechanics literature (28).

Material	Young's Modulus (MPa)
1	1012.5
2	802.90
3	58.462
4	52.641
5	15.309
6	6.767
7	2.698
8	1.166
9	0.439

**Table S1. Young's moduli of the materials in the gradient.** The materials used were digital combinations of commercial 3D printing materials offered by Stratasys, specifically VeroWhitePlus RGD835 (rigid) and TangoPlus FLX930 (flexible). Detailed information on these materials may be found on the Stratasys website ([http://www.stratasys.com/~media/Main/Secure/Material%20Specs%20MS/PolyJet-Material-Specs/Digital%20Materials\\_Datasheet-08-13.pdf](http://www.stratasys.com/~media/Main/Secure/Material%20Specs%20MS/PolyJet-Material-Specs/Digital%20Materials_Datasheet-08-13.pdf)).

### **Movie S1**

This movie depicts the animated simulation results, as in Fig. 2. The first sequence shows the evolution of body shape for the rigid top, gradient top, and flexible top robots as the volume of the gas inside the body expands. The second sequence compares the impact behavior of the same three cases.

### **Movie S2**

This movie presents the results of experimental testing, as in Fig. 3. The first sequence compares the impact behavior of the rigid top and gradient top robots. The second sequence depicts the robot performing a targeted jump off of an angled surface, and includes high-speed video of the takeoff. The final sequence shows the robot performing a directional jump on a flat surface.